Available online at www.sciencedirect.com
ScienceDirect
Journal of Nuclear Materials 366 (2007) 336–352
journal of nuclear materials
www.elsevier.com/locate/jnucmat

# Aging effects on microstructural and mechanical properties of select refractory metal alloys for space-reactor applications

Keith J. Leonard *, Jeremy T. Busby, Steven J. Zinkle

*Oak Ridge National Laboratory, Materials Science and Technology Division, P.O. Box 2008, Oak Ridge, TN 37831-6138, United States*

**Abstract**

Refractory alloys based on niobium, tantalum and molybdenum are potential candidate materials for structural applications in proposed space nuclear reactors. Long-term microstructural stability is a requirement of these materials for their use in this type of creep dominated application. Early work on refractory metal alloys has shown aging embrittlement occurring for some niobium and tantalum-base alloys at temperatures near 40% of their melting temperatures in either the base metal or in weldments. Other work has suggested microstructural instabilities during long-term creep testing, leading to decreased creep performance. This paper examines the effect of aging 1100 h at 1098, 1248 and 1398 K on the microstructural and mechanical properties of two niobium (Nb–1Zr and FS-85), tantalum (T-111 and ASTAR-811C) and molybdenum (Mo–41Re and Mo–47.5Re) base alloys. Changes in material properties are examined through mechanical tensile testing coupled with electrical resistivity changes and microstructural examination through optical and electron microscopy analysis.
Published by Elsevier B.V.

*PACS:* 89.30.Gg; 81.05.Bx; 81.40.Cd; 62.20.Hg; 62.20.Fe

## 1. Introduction

Phase stability and microstructural changes are key issues in understanding and predicting the long-term performance of refractory metal alloys at the high temperatures (>1000 K) required for space-reactor applications. The higher operating temperatures which may exclude the use of conventional or commercial alloys is needed to increase the thermodynamic efficiency of the power supply in order to minimize launch mass. Preliminary work has been conducted on the effects of long-term aging of refractory alloys in vacuum and lithium environments for select refractory alloys [1–5]. In some of these initial tests, decreases in bend ductility were reported for the T-111 alloy at 1313 K [3] and for the FS-85 alloy at 1255 K [5] after only 1000 h aging. However, to date there has not been a detailed characterization of aging effects or full characterization of the microstructures of candidate refractory metal alloys. Furthermore, little to no transmission electron microscopy has been performed on alloys in the annealed or aged conditions.

In this work thermal aging treatments following solution annealing have been performed at 1098, 1248 and 1398 K for 1100 h in inert gas to examine

* Corresponding author. Fax: +1 865 241 3650.
*E-mail address:* leonardk@ornl.gov (K.J. Leonard).

0022-3115/$ - see front matter Published by Elsevier B.V.
doi:10.1016/j.jnucmat.2007.03.025

both the upper operating temperature regime and a temperature range where detrimental effects on mechanical properties have been previously reported in some of the alloys. These aging treatments were chosen to complement radiation effects studies using the high flux isotope reactor (HFIR) to be discussed in a separate paper [6]. In this paper, the changes in electrical resistivity, microhardness and tensile properties of the six alloys: Mo–41Re, Mo–47.5Re, FS-85, Nb–1Zr, ASTAR-811C and T-111 are discussed and compared to observed microstructural changes following aging. The results obtained are preliminary, but offer an important first evaluation of alloy behavior in long-term applications, in addition to establishing areas where future work is needed.

## 2. Experimental

### 2.1. Refractory metal specimens

Sheet stock of the Mo–47.5Re, ASTAR-811C, T-111 and FS-85 alloys were provided by Pittsburgh Materials Technology Inc., and the Mo–41Re alloy was produced at ORNL by vacuum arc re-melting. The Nb–1Zr alloy was purchased from Cabot Supermetals, Inc. The measured chemical compositions of the alloys in the as-annealed condition are listed in Table 1.

Sheet tensile specimens of type SS-3 geometry ($0.76 \times 1.52 \times 7.62$ mm gauge and 25.4 mm overall length) were fabricated from the as-received material using Mo-wire electrical discharge machining (EDM) with water as the cooling fluid to minimize impurity pickup. Specimens were cut so that the gage length of the tensile samples was parallel to the rolling direction of the sheet material. Following cutting, samples were polished to a 32 or better finish, inspected and measured prior to thermal treatments and testing. In addition to the SS-3 samples, metallographic samples were also cut from the as-received material. After sample fabrication and prior to annealing, all samples were electrochemically cleaned for one minute in a solution of nitric acid, phosphoric acid, hydrofluoric acid and acetic acid.

Table 1
Measured composition of the alloys following annealing (in wt%)

| Alloy | Mo | Re | Ta | Nb | W | Zr | Hf |
|---|---|---|---|---|---|---|---|
| Mo–41Re | Bal. | 41.90 | – | – | – | – | – |
| Mo–47.5Re | Bal. | 47.18 | – | – | – | – | – |
| FS-85 | – | – | 26.85 | Bal. | 11.35 | 0.80 | – |
| Nb–1Zr[a] | – | – | – | Bal. | – | 0.95 | – |
| ASTAR-811C | – | 1.53 | Bal. | – | 8.35 | 0.037 | 0.96 |
| T-111 | – | – | Bal. | – | 8.69 | 0.037 | 2.01 |

[a] Alloy in the as-received, cold-worked condition.

### 2.2. Thermal treatments

All samples were annealed for 1 h in vacuum of $1.3 \times 10^{-4}$ Pa ($1 \times 10^{-6}$ torr) or better, with the specimens placed inside a Nb–1Zr box in the furnace to further reduce the potential for impurity pickup. The Mo-base alloys were annealed at 1773 K, the Ta-base alloys at 1883 K, the FS-85 samples at 1663 K, and the Nb–1Zr samples at 1835 K. Samples were furnace cooled at approximately 100 K/min in the first few minutes after which the cooling rate decreased asymptotically with time.

The aging treatments were conducted in parallel with irradiation experiments conducted at ORNL, the results of which will be presented separately [6]. Therefore, the SS-3 samples were loaded into pure Nb holders held in place with Mo springs similar to their irradiated counterparts. The Nb holders containing the tensile specimens along with Ta foil wrapped metallurgical samples were loaded into alumina tubes with alumina end-caps that were in turn placed in an alloy 600 tube and sealed with end caps. The superalloy capsules were welded shut under the same inert gas used in irradiation study: He for 1098 and 1248 K aging and Ne for the 1373 K aging. Prior to welding, repeated pumping and purging cycles were performed to ensure a purified atmosphere in the encapsulated cans. During each pump cycle a vacuum of approximately $1.3 \times 10^{-4}$ Pa ($1 \times 10^{-6}$ torr) was obtained. Leak checking of the sealed capsules was performed prior to aging in open air box furnaces at 1098, 1248 and 1398 K. Temperatures in the box furnace were monitored by thermocouples located near the sealed capsules. Aging treatments were for 1100 h.

Visual inspection of the samples following 1100 h aging at 1098 and 1248 K showed no signs of discoloration (oxidation). However, discoloration was observed on the Ta foil and Nb holders containing the samples in the 1398 K aging capsule. Further, discoloration was observed on ends of the grip sections of several SS-3 tensile bars that were nearest the open end of the Nb holders. The Ta and Nb-base alloys showed some tip discoloration, while the Mo alloy samples showed none. No measurable increase in sample weight was observed.

Chemical analysis of the annealed and aged refractory alloys was performed at Wah Chang through inert gas fusion techniques for oxygen and nitrogen, and by combustion analysis for carbon levels. The interstitial impurity elements in the alloys following 1 h anneal and 1100 h aging are presented in Table 2. Analysis of substitutional impurities (Al, B, Be, Co, Cr, Cu, Fe, Ni, Si and Ti) in the annealed and aged alloys was also performed, with values remaining below the detectable 50 wppm level. Analysis of the Nb–1Zr alloy was not included in this study, though interstitial levels of 22, 130 and 40 wppm were determined for C, O and N, respectively in the as-supplied material.

For both Mo–Re alloys, the impurity levels remain essentially unchanged after aging at all three temperatures with the exception of an increase in nitrogen content to 81 ppm of Mo–41Re after aging at 1398 K. However, this is still a relatively low interstitial level. The impurities in the FS-85 alloy are also essentially unchanged between the annealed and aged conditions. However, an increase in the oxygen level over the as-received was measured, though the source for chemical analysis was different between these conditions and could contribute to the measured differences. Chemical analysis also showed little change in the impurity values of ASTAR-811C and T-111 aged at 1098 and 1248 K. However, for the ASTAR-811C, the oxygen and nitrogen content increase significantly after aging at 1398 K. The T-111 also shows higher nitrogen content after aging at 1398 K, although the oxygen content is unchanged from the annealed condition.

The samples provided for chemical analysis were taken from both the gauge regions of the tensile tested samples and from unused metallographic samples that showed no visible discoloration. The apparent interstitial pickup for ASTAR-811C and T-111, for example, may be the result of a surface film still present on the sample (as the techniques do not discriminate where the oxygen is located). A simple analysis indicates that a 150 mg sample of a Ta-base alloy (at 0.8 mm thick) needs to have only 1% of the surface area covered with a 26 μm oxide layer to have 290 ppm of oxygen. Nonetheless,

Table 2
Chemical impurity analysis following 1 h anneal and 1100 h aging treatments

| Alloy | Condition | C (wt ppm) | N (wt ppm) | O (wt ppm) | H (wt ppm) |
|---|---|---|---|---|---|
| Mo–41Re | Annealed 1 h at 1773 K[a] | <20 | <20 | <50 | <3 |
| | Aged 1100 h at 1098 K | 27 | <20 | <50 | <3 |
| | Aged 1100 h at 1248 K | <20 | <20 | <50 | <3 |
| | Aged 1100 h at 1398 K | <20 | 81 | <50 | <3 |
| Mo–47.5Re | As-received[b] | 49 | 27 | 65 | – |
| | Annealed 1 h at 1773 K | 32 | <20 | <50 | <3 |
| | Aged 1100 h at 1098 K | 35 | <20 | <50 | <3 |
| | Aged 1100 h at 1248 K | 32 | <20 | <50 | <3 |
| | Aged 1100 h at 1398 K | <20 | <20 | <50 | <3 |
| FS-85 | As-received[b] | <50 | 56 | 120 | – |
| | Annealed 1 h at 1663 K | 22 | 56 | 280 | <3 |
| | Aged 1100 h at 1098 K | 27 | 64 | 290 | <3 |
| | Aged 1100 h at 1248 K | 22 | 49 | 140 | <3 |
| | Aged 1100 h at 1398 K | 30 | 58 | 270 | <3 |
| ASTAR-811C | As-received[b,c] | 230 | 15 | 75 | – |
| | Annealed 1 h at 1883 K | 254 | <20 | <50 | <3 |
| | Aged 1100 h at 1098 K | 265 | 60 | <20 | <3 |
| | Aged 1100 h at 1248 K | 258 | 60 | <20 | <3 |
| | Aged 1100 h at 1398 K | 248 | 210 | 290 | <3 |
| T-111 | As-received[b,c] | 45 | 27 | 65 | – |
| | Annealed 1 h at 1883 K | 108 | 25 | 110 | <3 |
| | Aged 1100 h at 1098 K | 86 | <20 | 70 | <3 |
| | Aged 1100 h at 1248 K | 81 | <20 | 120 | <3 |
| | Aged 1100 h at 1398 K | 78 | 110 | 150 | <3 |

[a] Material received in the as-annealed condition.
[b] Analysis provided by PMTI.
[c] Analysis in 1960/1970.

any observed changes in mechanical properties for the Ta-alloys aged at 1398 K must be viewed with this apparent impurity pickup in mind.

### 2.3. Metallography

Pieces from the annealed and aged metallographic samples were polished and examined in a Philips XL30-FEG scanning electron microscope (SEM). The metallographic samples were then etched and examined by optical microscopy (OM). Samples for transmission electron microscopy (TEM) were cut by EDM and polished to less than 0.25 mm thickness prior to jet-polishing with an electrolyte of 10 vol.% $H_2SO_4$ + 4% HF + 14% Butoxy Ethanol in methanol. Samples were examined in both a Philips Tecnai T20 and CM200 FEG microscopes equipped with energy dispersive X-ray spectrometers (EDS).

Multiple hardness measurements were made at room temperature on the annealed and aged tensile specimens of each alloy using a Buehler Micromet 3 hardness indenter equipped with a Vickers indenter tip using a 1 kg load, with a dwell time of 15 s. Typically, one specimen was analyzed for each alloy/aging combination. All indents were made on the grip regions of the SS-3 tensile specimens, well away from the gage length so that later tensile tests were not influenced.

### 2.4. Electrical resistivity

Electrical resistivity was measured at room temperature using a four-point probe technique on the standard SS-3 tensile specimens of each alloy in the as-annealed and aged conditions, in accordance with ASTM standard B193-87 [7]. The measured voltage drop was readily converted to resistivity with room temperature (294.6 K) chosen as the reference temperature for the calculation. The resistivity is calculated from the measured voltage drop using:

$$\rho_{294.6}(\text{n}\Omega\text{-m}) = \frac{(V \times A)}{(I \times L)(1 + \alpha(T_m - 294.6))} \qquad (1)$$

where $\rho_{294.6}$, resistivity in nanoOhm-m at the reference temperature of 294.6 K; $V$, measured voltage at the measurement temperature (nanoVolts); $A$, cross-sectional area of sample ($m^2$); $I$, applied current (0.1 A); $L$, distance between inner electrodes (0.00646 m); $\alpha$, temperature coefficient of electrical resistivity; $T_m$, temperature of measurement (K).

For each specimen, the cross-sectional area was measured using a calibrated micrometer with 1 μm or better resolution. The width of the gage section is measured at the center of the gage section and the specimen thickness is measured at two locations along the gage length. The temperature was measured before and after electrical measurements on each set of specimens. The temperature coefficient of electrical resistivity, $\alpha$, was selected as $0.0044\ K^{-1}$ for the Mo-alloys which was the value for pure Mo ($\alpha$ for pure Re = $0.0045\ K^{-1}$) [8]. Similarly, the values of $\alpha$ for the Ta and Nb-base alloys were 0.0035 and $0.0026\ K^{-1}$, taken from the pure metal values, respectively.

### 2.5. Tensile testing

Tensile testing was performed on the as-annealed and aged SS-3 specimens and follows ASTM standard E8-04 [9]. Yield stress (YS), ultimate tensile stress (UTS), and uniform and total elongation were determined for each test. Tests at room temperature and above were performed using a United Technology System SFM-10, equipped with a Thermal Technology vacuum furnace. Tensile tests were performed at a crosshead speed of 0.0076 mm/s (0.018 in/min), corresponding to a nominal strain rate of $\sim 0.001\ s^{-1}$. Testing of the aged samples was performed at the same targeted temperatures as their companion irradiated samples (1073, 1223, or 1373 K). Temperatures were measured using a type-C thermocouple positioned within 2 mm of the gauge section. Room temperature tests were conducted in air, while elevated temperature testing was in vacuum. Vacuum pressure during testing was maintained at $2 \times 10^{-6}$ torr or lower.

## 3. Results and discussion

Measurements of electrical resistivity and hardness were performed on specimens of all alloys following 1 h anneals and 1100 h aging treatments at 1098, 1248 and 1398 K. Changes in electrical resistivity and hardness were observed in most of the alloys between the as-annealed and aged conditions. The changes in electrical resistivity of the refractory alloys following aging is illustrated in Fig. 1 with values presented in Table 3. The annealing of the as-received cold-worked alloys produced minimal changes in resistivity indicating that grain boundaries and dislocations contribute little to the

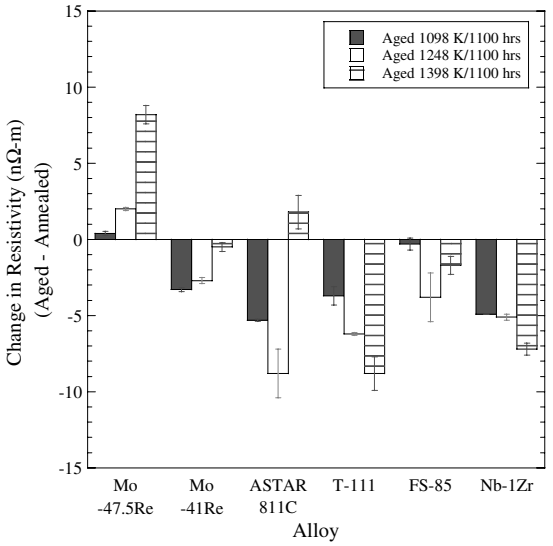


Fig. 1. Comparison of the average change in resistivity between aged and annealed conditions for individual alloy specimens. The error bars represent the standard deviation of the mean for the associated number of measurements.

resistivity and that there were no pronounced changes in precipitate type, structure or distribution. The changes in electrical resistivity values do indicate that there are either solute redistributions or microstructural changes occurring during aging. It should be pointed out that the values of resistivity listed in Table 3 represent the averaged values of all samples tested for a given condition, while the changes in resistivity illustrated in Fig. 1 are a more precise representation of the average change in resistivity between the annealed and aged conditions occurring for a given set of samples.

Significant changes in resistivity between the as-annealed and aged conditions were found to occur in several alloys. Resistivity changes of 5–10 nΩ-m are as large as would be expected to occur in the refractory alloys without a significant increase in impurity level [10]. For the Mo–Re alloys, electrical resistivity was observed to trend in opposite directions with increasing aging temperature. Large resistivity decreases were observed for both Ta-base alloys. Though the increase in resistivity for ASTAR-811C aged at 1398 K may have been caused by the increases in O and N, further decreases in resistivity were observed for the 1398 K aged T-111 despite the increase in N level. A similar trend in electrical resistivity and hardness with aging temperature was observed for Nb–1Zr as that of T-111.

The room temperature hardness measurements on the as-received, annealed, and thermally aged alloys are listed in Table 4. The results for all conditions are compared in Fig. 2 for the refractory alloy candidates. Solution annealing produced a significant reduction in hardness from the as-received value for all tested alloys, as expected due to a reduction in dislocation density from the initial cold-worked condition. Cold-worked hardness values were not available for the Mo–41Re alloy since this material was received in the annealed condition. Significant increases in hardness on aging were observed for Mo–47.5Re at 1248 and 1398 K and for Nb–1Zr at 1098 K, while losses in hardness were observed for ASTAR-811C at 1098 and 1248 K.

Although electrical resistivity and hardness provides a simple method for evaluating the amount of change resulting from thermal aging, they do not provide information regarding the specific microstructural changes that can affect the mechanical properties of the alloys. Electron microscopy techniques provide this detailed look at microstructural changes; something which has not been performed to date for most of these materials. Microstructural information is now presented for each alloy group.

### 3.1. Mo-base alloys

In general, the resistivity of Mo–41Re and −47.5 Re agree well with the reported literature values of 202 nΩ-m at 373 K and 193 nΩ-m at 293 K [11], respectively. For the Mo–41Re alloy, a decrease in electrical resistivity from the as-annealed value was measured with decreasing aging temperature (Fig. 1 and Table 3); with the averaged value of resistivity of the 1398 K aged material close to that of the as-annealed condition. These changes correlated with increases in hardness with decreasing aging temperature and may be related to the distributions of interstitial solute in the alloy. Examination of the annealed and aged Mo–41Re samples by OM revealed equiaxed grains with a mean grain diameter of 24 μm for all conditions. Though the nominal composition of the Mo–41Re alloy lies just inside the two-phase αMo + σ field at lower temperatures (Fig. 3) [12], examination of all the annealed and aged materials by electron microscopy revealed no evidence of precipitation. Images of the 1098 K aged Mo–41Re taken from OM and TEM are shown in Fig. 4, with a representative selected area

Table 3
Resistivity measurements on the as-received, annealed and aged refractory alloys

| Alloy | Condition | Number of samples tested | Resistivity[b] (nΩ-m) |
|---|---|---|---|
| Mo–41Re | Annealed, 1 h at 1773 K (as-received) | 40[a] | 184.6 ± 0.4 |
| | Annealed + Aged, 1100 h at 1098 K | 3 | 180.4 ± 1.6 |
| | Annealed + Aged, 1100 h at 1248 K | 3 | 181.1 ± 0.9 |
| | Annealed + Aged, 1100 h at 1398 K | 3 | 184.0 ± 0.9 |
| Mo–47.5Re | As-received | 39[a] | 200.5 ± 0.4 |
| | Annealed, 1 h at 1773 K | 39[a] | 198.0 ± 0.7 |
| | Annealed + Aged, 1100 h at 1098 K | 3 | 194.9 ± 0.2 |
| | Annealed + Aged, 1100 h at 1248 K | 3 | 196.9 ± 1.7 |
| | Annealed + Aged, 1100 h at 1398 K | 3 | 202.9 ± 1.3 |
| FS-85 | As-received | 59[a] | 203.0 ± 0.3 |
| | Annealed, 1 h at 1643 K | 39[a] | 200.4 ± 0.5 |
| | Annealed + Aged, 1100 h at 1098 K | 3 | 199.8 ± 0.9 |
| | Annealed + Aged, 1100 h at 1248 K | 3 | 199.5 ± 3.1 |
| | Annealed + Aged, 1100 h at 1398 K | 3 | 196.4 ± 1.3 |
| Nb–1Zr | As-received | 60[a] | 164.5 ± 0.2 |
| | Annealed, 1 h at 1835 K | 42[a] | 164.5 ± 0.3 |
| | Annealed + Aged, 1100 h at 1098 K | 3 | 159.2 ± 0.3 |
| | Annealed + Aged, 1100 h at 1248 K | 3 | 161.3 ± 0.2 |
| | Annealed + Aged, 1100 h at 1398 K | 3 | 158.2 ± 0.2 |
| ASTAR-811C | As-received | 40[a] | 205.1 ± 0.3 |
| | Annealed, 1 h at 1883 K | 40[a] | 204.4 ± 0.4 |
| | Annealed + Aged, 1100 h at 1098 K | 3 | 198.0 ± 0.6 |
| | Annealed + Aged, 1100 h at 1248 K | 3 | 195.4 ± 1.4 |
| | Annealed + Aged, 1100 h at 1398 K | 3 | 207.4 ± 1.1 |
| T-111 | As-received | 40[a] | 201.1 ± 0.2 |
| | Annealed, 1 h at 1883 K | 40[a] | 203.5 ± 0.3 |
| | Annealed + Aged, 1100 h at 1098 K | 3 | 199.5 ± 1.0 |
| | Annealed + Aged, 1100 h at 1248 K | 3 | 196.6 ± 0.3 |
| | Annealed + Aged, 1100 h at 1398 K | 3 | 193.7 ± 1.0 |

[a] Includes samples used in separate irradiation testing work.
[b] Five measurements taken on each specimen, with the error listed as the standard deviation of the mean.

diffraction (SAD) pattern of the αMo[1 1 0] zone axis. The zone axis pattern contains diffracting intensities from only the bcc αMo solid solution, with no signs of precipitation, decomposition or ordering in the solid solution. Work by Nemoto et al. [13] on Mo–Re alloys, also observed no evidence of precipitation in Mo–41Re aged for 720 h at temperatures up to 1073 K. The sluggish kinetics at these temperatures suggests some degree of stability, though enhanced precipitate formation may occur under radiation environments.

Differences were not observed in the tensile properties of Mo–41Re between the as-annealed and the 1098 and 1248 K aged materials (Table 5). However, an increase in the yield and ultimate tensile strengths of the 1398 K aged material over the as-annealed was measured. A slight reduction in the uniform elongation was observed for the 1398 K sample, though these properties represent only one test. This may have been the result of the slight increase in N level in the alloy measured by chemical analysis (Table 2), though the level of N is still relatively low and may represent normal scatter in chemical analysis tests. Nevertheless, adequate uniform and total elongation values are observed. The tensile properties of Mo–41Re measured in this study were in excellent agreement with those of Leonhardt et al. [14], which also reported a slight reduction in uniform elongation of the as-annealed material tested at 1475 K.

The changes in the electrical resistivity and mechanical properties following 1100 h aging were found to correlate directly with precipitate development in the Mo–47.5Re alloy. Similar to Mo–41Re, no statistically significant change was found in the 24 μm average grain size of the solid solution,

Table 4
Results of hardness measurements on as-received, annealed, and aged specimens

| Alloy | Condition | Hardness[a] (kg/mm$^2$) |
|---|---|---|
| Mo–41Re | Annealed, 1 h at 1773 K | 321 ± 5 |
| | Annealed + Aged, 1100 h at 1098 K | 340 ± 6 |
| | Annealed + Aged, 1100 h at 1248 K | 323 ± 4 |
| | Annealed + Aged, 1100 h at 1398 K | 320 ± 4 |
| Mo–47.5Re | Annealed, 1 h at 1773 K | 334 ± 2 |
| | Annealed + Aged, 1100 h at 1098 K | 342 ± 5 |
| | Annealed + Aged, 1100 h at 1248 K | 376 ± 5 |
| | Annealed + Aged, 1100 h at 1398 K | 361 ± 6 |
| FS-85 | Annealed, 1 h at 1643 K | 190 ± 2 |
| | Annealed + Aged, 1100 h at 1098 K | 208 ± 2 |
| | Annealed + Aged, 1100 h at 1248 K | 184 ± 1 |
| | Annealed + Aged, 1100 h at 1398 K | 187 ± 1 |
| Nb–1Zr | Annealed, 1 h at 1835 K | 91 ± 1 |
| | Annealed + Aged, 1100 h at 1098 K | 116 ± 6 |
| | Annealed + Aged, 1100 h at 1248 K | 74 ± 1 |
| | Annealed + Aged, 1100 h at 1398 K | 82 ± 1 |
| ASTAR-811C | Annealed, 1 h at 1883 K | 289 ± 2 |
| | Annealed + Aged, 1100 h at 1098 K | 260 ± 6 |
| | Annealed + Aged, 1100 h at 1248 K | 261 ± 2 |
| | Annealed + Aged, 1100 h at 1398 K | 301 ± 5 |
| T-111 | Annealed, 1 h at 1883 K | 253 ± 3 |
| | Annealed + Aged, 1100 h at 1098 K | 241 ± 4 |
| | Annealed + Aged, 1100 h at 1248 K | 236 ± 3 |
| | Annealed + Aged, 1100 h at 1398 K | 235 ± 1 |

[a] A minimum of five measurements were taken on each specimen at room temperature, with errors listed as the standard deviation of the mean.

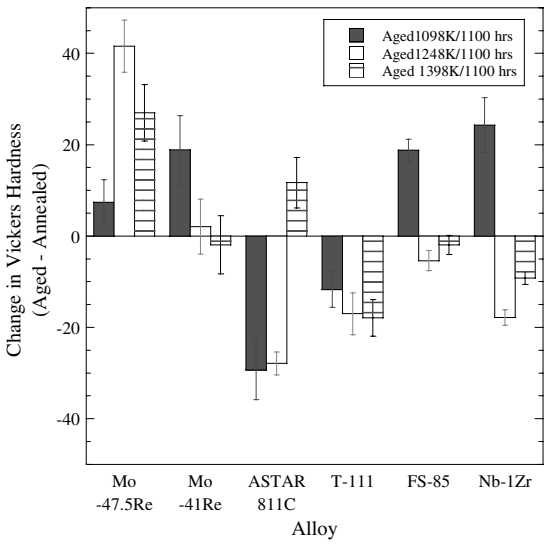


Fig. 2. Comparison of the change in hardness after aging treatment for each alloy. The error bars represent the standard deviation of the mean for the associated number of measurements.

although, this is not expected given that aging temperatures were between 0.3 and 0.5 of the melting temperatures for the alloys. Examination of the

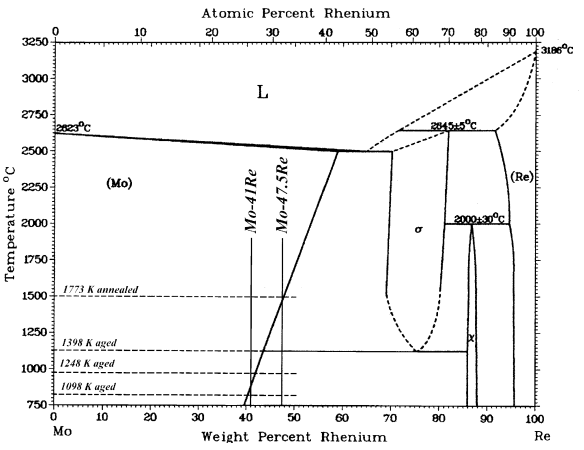


Fig. 3. The Mo–Re binary diagram from reference [12], with the alloy and aging conditions that were examined in this study marked.

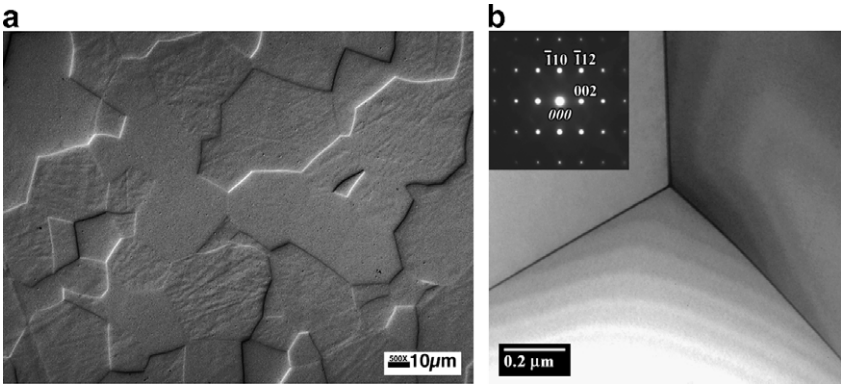


Fig. 4. (a) Optical and (b) TEM images of single phase solid solution (α-Mo) microstructure of Mo–41Re aged 1100 h at 1098 K. Image (b) shows a clean grain boundary tri-junction with the insert showing the αMo[1 1 0] SAD pattern.

Table 5
Tensile properties of Mo-base alloys

| Alloy | Test temperature (K) | Condition | # of Tests | YS (MPa) | UTS (MPa) | Uniform elongation (%) | Total elongation (%) |
|---|---|---|---|---|---|---|---|
| Mo–41Re | 295 | Annealed | 1 | 769 | 900 | 17.2 | >25 |
| | 1073 | Annealed | 1 | 303 | 503 | 17.9 | 30 |
| | | Aged 1098 K | 1 | 294 | 500 | 19.2 | 30.6 |
| | 1223 | Annealed | 1 | 275 | 393 | 16.8 | 39 |
| | | Aged 1248 K | 1 | 265 | 398 | 16.8 | 35.1 |
| | 1373 | Annealed | 1 | 228 | 275 | 11.7 | 50.5 |
| | | Aged 1398 K | 1 | 241 | 300 | 9.4 | 62.3 |
| Mo–47.5Re | 295 | Annealed | 1 | 561 | 893 | 17.4 | 19.9 |
| | 1073 | Annealed | 1 | 270 | 510 | 15.3 | 25.0 |
| | | Aged 1098 K[a] | 3 | 277 | 515 | 18.2 | 27.3 |
| | 1223 | Annealed | 1 | 300 | 464 | 15.1 | 29.6 |
| | | Aged 1248 K[a] | 2 | 270 | 462 | 17.4 | 37.2 |
| | 1373 | Annealed | 1 | 223 | 326 | 14.5 | 62.9 |
| | | Aged 1398 K[a] | 2 | 257 | 346 | 8.2 | 33.8 |

[a] Averaged values from multiple tensile tests.

1773 K annealed structure of Mo–47.5Re by TEM revealed the presence of σ-phase particles randomly distributed along the grain boundaries and in grain interiors (Fig. 5(a)). Two-phase structures were also reported by Shields [15] following 1 h anneal of Mo–47.5Re at 1773 K, with traces of the σ-phase remaining following 2.7 h annealing at 1873 K having also been reported [16].

Aging Mo–47.5Re at 1398 K produced a nearly continuous precipitation of the σ-phase along grain boundaries (Fig. 5(b)). Due to the σ[1 0 0]||αMo[1 0 0] orientation relationship in the growth of σ particles [17], a more angular and faceted particle morphology appears in the 1398 K aged material than in the as-annealed. Similar to the 1398 K aged material, the 1248 K aged samples showed nearly complete grain boundary coverage by precipitates throughout (Fig. 5(c)). However, several features separate the 1248 K aged material from that of the 1398 K aged condition. These include an apparent decrease in volume fraction of the grain boundary phase and lack of precipitation in the grain interiors. The grain boundary precipitate structure was identified by TEM analysis (Fig. 6) as the cubic structured χ-phase, accounting for the change observed in volume fraction between the 1248 and 1398 K samples due to compositional changes. The appearance of the χ-phase and the absence of σ particles correlate with the aging of the sample in the αMo + χ phase field based on

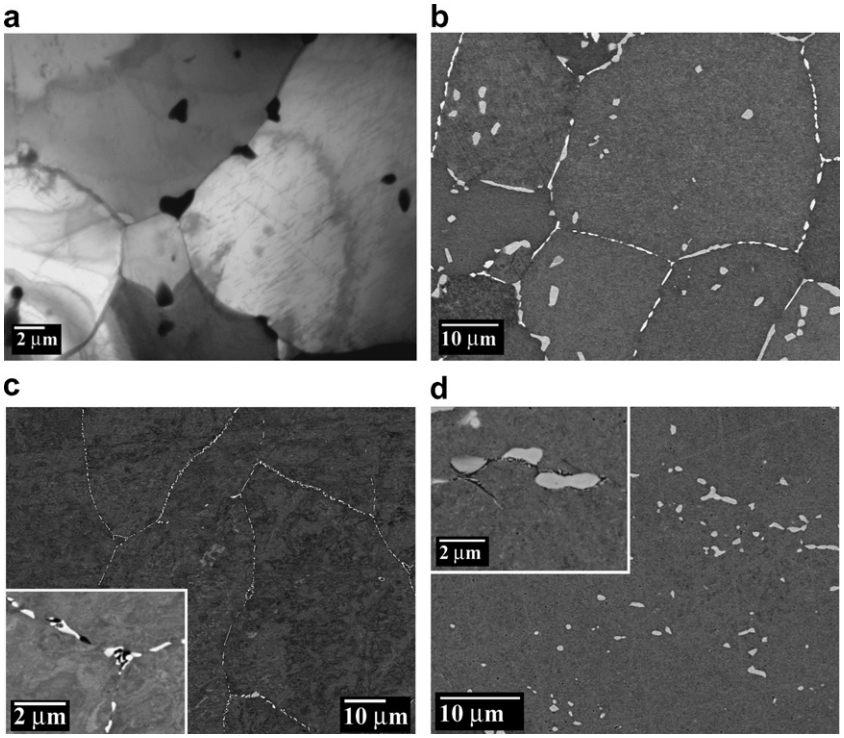


Fig. 5. (a) TEM micrograph of Mo–47.5Re annealed 1 h at 1773 K. Back-scatter electron images of the alloy aged 1100 h at (b) 1398 K, (c) 1248 K, and (d) 1098 K. Inserts show higher magnification images of the particles.

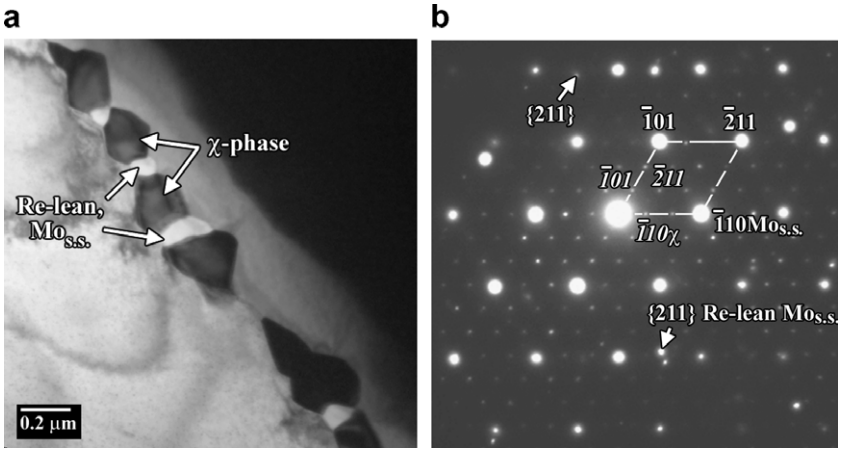


Fig. 6. (a) TEM micrograph showing χ-phase precipitation and the development of Re-lean solid solution ($Mo_{s.s.}$) grains along a grain boundary in Mo–47.5Re aged 1100 h at 1248 K. (b) SAD pattern showing the $\chi[1\,1\,1]\|\alpha Mo[1\,1\,1]$ orientation relationship with χ-phase reflections at $\sim 1/3\{hkl\}$ of the αMo phase.

the Mo–Re phase diagram shown in Fig. 3 [12]. However, this contradicts earlier work [16] that showed an extension of the σ phase field to temperatures below 1398 K. The morphology of the χ-phase and its direct one-to-one orientation relationship with the αMo solid solution are shown in more detail in the TEM images of Fig. 6. In addition to the χ-phase particles at the grain boundary,

grains of solid solution with a Re-lean composition (below 18 wt%) were also observed and account for the dark contrasting features observed under back-scatter electron imaging of the 1248 and 1098 K aged materials. Unlike the 1248 K aged sample which showed no σ-phase particles in the microstructure, sluggish diffusion kinetics of the 1098 K aging left remnant σ particle from the as-annealed condition (Fig. 5(d)). Closer examination of the grain boundaries by SEM and TEM revealed χ-phase precipitation similar to that occurring at 1248 K in addition to Re-lean grains, but with particle sizes typically below 100 nm.

Despite the small amount of χ formation in the 1098 K aged Mo–47.5 Re, the dominant microstructural features consisted of the remnant σ particles from the anneal and therefore no significant change in tensile properties was observed over that of the as-annealed material (Table 5). The precipitation of the χ-phase may have been the cause for the decrease in electrical resistivity of the 1098 K aged material over that of the as-annealed condition. The increase in hardness of the 1098 K aged Mo–47.5Re is attributed to that particular sample having a slightly greater tensile strength over the as-annealed material. While the 1248 K aged Mo–47.5Re alloy showed extensive grain boundary development of the χ-phase and a higher hardness over the as-annealed condition, preliminary tensile data shows no loss of ductility. Though the 1248 K aged material shows a reduced yield strength compared to the as-annealed material tested at 1223 K, the yield strengths of the two conditions remain at levels near the 1098 K aged and as-annealed materials tested at 1073 K. The measured UTS values of the annealed Mo–47.5Re of this study are in close agreement with those of Leonhardt et al. [14], while YS are considerably lower than the literature values. However, this may be due to differences in processing treatment leading to differences in σ-phase distributions. A decrease in the uniform ductility occurred in the 1398 K aged material as a result of the substantial precipitation of the σ-phase along the grain boundaries of the solid solution grains. However, total elongation remains high at 1373 K. The deformation mechanisms and mechanics that allow for the high tensile elongations in the χ-phase precipitated 1248 K aged sample are not understood at this time, nor is it known how the extensive grain boundary precipitation in Mo–47.5Re affects the fracture toughness of the alloy.

### 3.2. Nb-base alloys

No direct comparisons of electrical resistivity for Nb–1Zr and FS-85 could be made with literature values. However, values of 164 and 204 nΩ-m at room temperature for pure Nb and Nb–Ta alloys [11], respectively, are in good agreement with the measured values in this study (Fig. 1 and Table 3). Both the Nb-base alloys, FS-85 and Nb–1Zr, showed changes in electrical resistance and mechanical properties associated with microstructural changes occurring during the 1100 h aging. A decrease in electrical resistivity from the as-annealed condition was observed at all aging conditions with the largest decreases occurring at 1248 and 1398 K for FS-85 and Nb–1Zr, respectively. Similar behavior was observed between the two alloys with respect to hardness changes following aging (Fig. 2 and Table 4), with an increase in hardness following 1098 K aging and decreases after aging at higher temperatures.

Annealing of FS-85 for 1 hr at 1643 K resulted in equiaxed grains containing $ZrO_2$ particles of 0.2–0.3 μm in size distributed sparsely and randomly throughout the grains. The appearance of the $ZrO_2$ particles may have been the result of the increase in oxygen impurity over the as-received material, suggesting that saturation of oxygen in the matrix was exceeded. Aging for 1100 h between 1098 and 1398 K did not produce a change in the 10 μm grain size of the solid solution grains, or produce an observable change in the size or distribution of the $ZrO_2$ particles from the as-annealed condition. Examples of the 1248 and 1398 K aged microstructures observed through back-scatter electron imaging are shown in Fig. 7. The primary change occurring in the microstructures of the aged samples is related to the precipitation of Zr-rich particles at the grain boundaries. The size of these particles, as measured from multiple TEM images at different locations in the samples and at different magnifications, increased from an average of 4.4 nm to 42.5 nm in the 1098 and 1248 K aged materials, with area particle densities of $2 \times 10^{15}$ and $5 \times 10^{14}$ $m^{-2}$ respectively. Aging at 1398 K produced a very sparse distribution of particles at the grain boundaries, but with particle sizes of up to 200 nm observed. Examples of grain boundary precipitation in the 1248 and 1398 K aged FS-85 are presented in Fig. 8. The particles developed along the grain boundaries in all of the aging conditions differ in structure than that of the monoclinic $ZrO_2$ particles

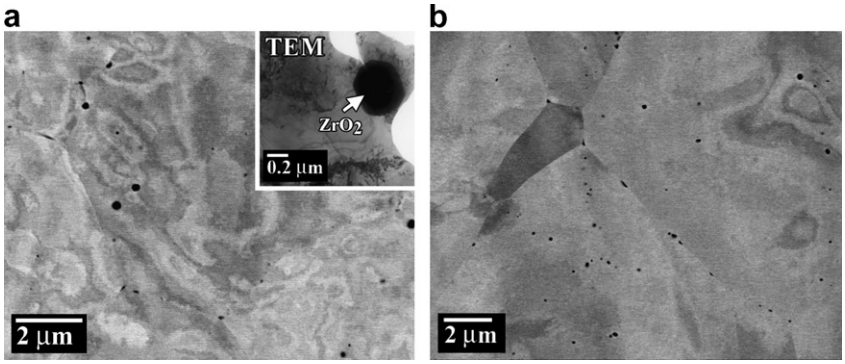


Fig. 7. Back-scatter SEM images of FS-85 aged 1100 h at (a) 1248 and (b) 1398 K, with insert in (a) showing a TEM image of a representative $ZrO_2$ particle, similar to particles observed in the alloy following all thermal treatments.

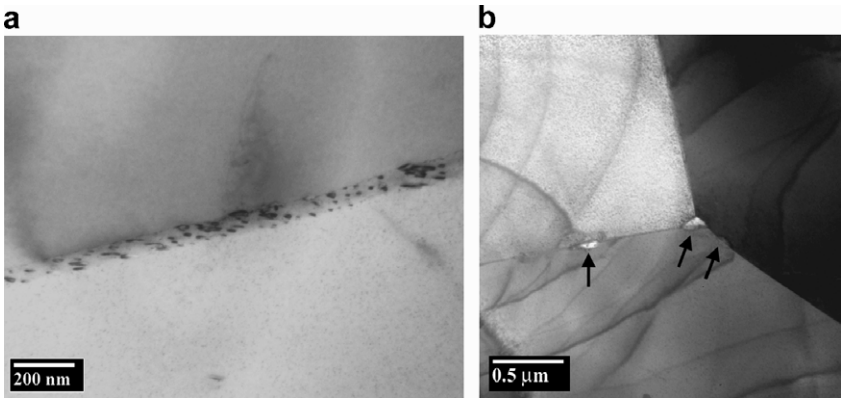


Fig. 8. TEM micrographs of Zr-rich precipitates at grain boundaries in FS-85 aged 1100 h at (a) 1248 K and (b) 1398 K. The boundary in (a) is highly tilted relative to the beam to illustrate the fine particle size and distribution, while that of (b) is near parallel.

developed on annealing. These grain boundary particles have the cubic, *Fm3m* structure, as determined through convergent beam electron diffraction analysis and an approximate lattice constant of 0.4578 nm as averaged over multiple diffraction vectors on the SAD patterns. A more in-depth analysis of the aged microstructures will be addressed in a later paper.

As shown earlier in Figs. 1 and 2, the largest negative change in electrical resistivity and hardness of FS-85 occurred from aging at 1248 K, suggesting a greater redistribution of solute elements from the solid solution at that temperature than at the others. While tensile test data for FS-85 is preliminary (Table 6), a significant loss in ductility was observed in the 1248 K aged sample compared to the as-annealed material tested at the same temperature. Though uniform elongation of the 1098 and 1398 K aged material show some reduction, total elongation is still around 20%. The tensile values of as-annealed FS-85, match closely with reference values compiled from recrystallized material [18,19].

A limited database exists for the effects of aging on the mechanical properties of FS-85. Lessmann and Gold [5] reported an increase in the bend test ductile-to-brittle transition temperatures (DBTT) for FS-85 aged at 1255 K for 1000 h or greater, while aging at 1088 K produced no increase. Their study also demonstrated an increase in DBTT on aging at 1422 K, but for times greater than 5000 h. Similar effects were also observed in weldments, where embrittlement occurred upon aging at 1255 K for over 100 h, but could be alleviated by annealing at 1588 K for as little as 1 h [5,20]. Embrittlement was not observed in tensile tests of FS-85 aged 1000 h between 1089 and 1589 K by Frank [21]. However, tensile testing was conducted at room temperature and at a strain rate approximately 12 times slower than used in this study. It is also worthwhile to note that similar embrittlement effects were observed by

Table 6
Tensile properties of Nb-base alloys

| Alloy | Test temperature (K) | Condition | # of Tests | YS (MPa) | UTS (MPa) | Uniform elongation (%) | Total elongation (%) |
|---|---|---|---|---|---|---|---|
| FS-85 | 295 | Annealed[a] | 2 | 504 | 595 | 17.4 | 32.0 |
| | 1073 | Annealed | 1 | 254 | 392 | 13.8 | 25.6 |
| | | Aged 1098 K | 1 | 287 | 365 | 8.8 | 19.2 |
| | 1223 | Annealed | 1 | 223 | 354 | 12.0 | 23.0 |
| | | Aged 1248 K | 1 | 161 | 207 | 2.3 | 3.0 |
| | 1373 | Annealed | 0 | | | | |
| | | Aged 1398 K | 1 | 158 | 289 | 5.3 | 22.6 |
| Nb–1Zr | 295 | Annealed | 1 | 185 | 281 | 18.6 | 34.6 |
| | 1073 | Annealed | 1 | 103 | 185 | 15.4 | 23.6 |
| | | Aged 1098 K | 1 | 161 | 252 | 3.6 | 11.9 |
| | 1223 | Annealed | 1 | 89 | 197 | 13.2 | 24.4 |
| | | Aged 1248 K[a] | 2 | 119 | 150 | 7.4 | 12.3 |
| | 1373 | Annealed | 0 | | | | |
| | | Aged 1398 K | 0 | | | | |

[a] Averaged values from multiple tests.

Stephens in Cb-752 (Nb–9.8 W–1Zr) aged 1000 h at 1175 K, but not at 1098 or 1248 K [1,3]. The reduced embrittlement temperature of Cb-752 may be attributed to the lower homologous temperature than FS-85 due to the lack of Ta in the alloy.

Unlike the annealed microstructure of FS-85, the 1835 K anneal of Nb–1Zr appears to have been sufficiently high to dissolve the $ZrO_2$ particles into the solid solution. Examination of the as-annealed microstructure by optical and electron microscopy showed dislocation and precipitate-free, equiaxed grains with a mean diameter of 70 μm. Grain sizes did not change during 1100 h aging at any temperature. While a decrease in the electrical resistivity (Fig. 1) and a significant increase in hardness (Fig. 2) occurred for aging at 1098 K, OM and SEM examination of the material was unable to reveal any changes in microstructure from the as-annealed condition. The change in resistivity and hardness correlate with a significant increase in tensile strengths over the as-annealed condition (Table 6). Though uniform elongation was 3.6%, total elongation remains over 10% with the fracture surfaces of the sample exhibiting ductile failure. Though examination of the aged Nb–1Zr material by TEM examination is required, the changes in electrical and mechanical properties suggest fine scale precipitation has occurred. Examination of the 1248 and 1398 K aged Nb–1Zr by SEM (Fig. 9) revealed intragranular and grain boundary precipitation development with increasing aging temperature. Further reduction in the electrical resistivity and a decrease in hardness relative to the as-annealed condition was measured following aging of Nb–1Zr at 1248 and 1398 K. While preliminary tensile test data extends to only the 1248 K aged material, a significant increase in the materials yield strength is observed in tests conducted on the 1248 K aged material at 1223 K. However, the aged material did not show the same

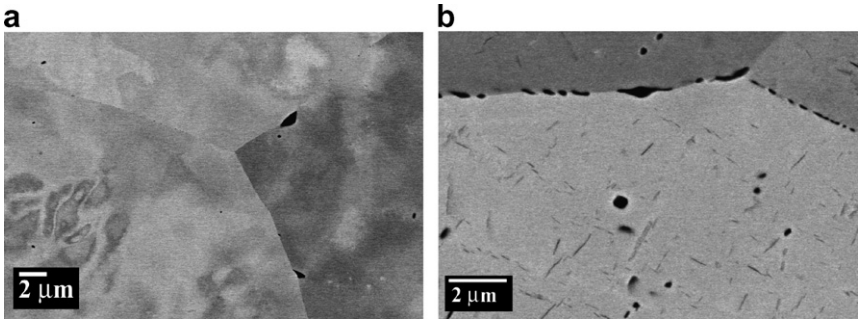


Fig. 9. Back-scatter SEM images of Nb–1Zr following 1100 h aging at (a) 1248 and (b) 1398 K.

level of work hardening as that of the as-annealed condition. Increasing the aging temperature to 1398 K produced a further growth of precipitates in Nb–1Zr (Fig. 9(b)), with what appears to be plate shaped intragranular particles with a defined orientation relationship to the matrix yet to be determined by TEM analysis. Coarsening of precipitate particles with aging temperature appears to be contributing to the observed decrease in electrical resistivity with aging temperature. Available reference data on aged Nb–1Zr, showed no change in bend-test DBTT for material aged 1000 h at temperatures between 973 and 1298 K [1].

### 3.3. Ta-base alloys

A trend of decreasing electrical resistance with increasing aging temperature was observed for T-111 (Fig. 1 and Table 3), which correlated with decreasing hardness values of the alloy (Fig. 2 and Table 4). Though ASTAR-811C showed decreases in resistivity and hardness upon aging at 1098 and 1248 K, increases in these test values over the as-annealed condition were measured following aging at 1398 K. The averaged resistivity values of T-111 in this study following the various treatments is below the 217 nΩ-m value reported in literature [22], but are within 10% of each other. No comparison data could be found for ASTAR-811C.

The as-annealed microstructure of ASTAR-811C revealed a slightly less uniform grain size distribution than that appearing in the previously discussed alloys, but mean grain diameters of 14 μm were measured for both the as-annealed and aged materials. Intragranular and grain boundary precipitation was observed in OM of the as-annealed material (Fig. 10(a)). Though unconfirmed, these particles are likely a mixture of $HfO_2$ and $Ta_2C$. As will be shown later, $HfO_2$ particles of 0.3 μm and less were present in T-111 following the same annealing conditions. In addition, $Ta_2C$ particles were observed in ASTAR-811C by Ammon et al. [23] in material helium quenched (~700 K/min.) from 2255 K.

Aging of ASTAR-811C for 1100 h produced similar results at 1098 and 1248 K. In addition to random and sparsely distributed intragranular particles of $Ta_2C$ and $HfO_2$ of approximately 0.3 μm size, grain boundary precipitation of $Ta_2C$

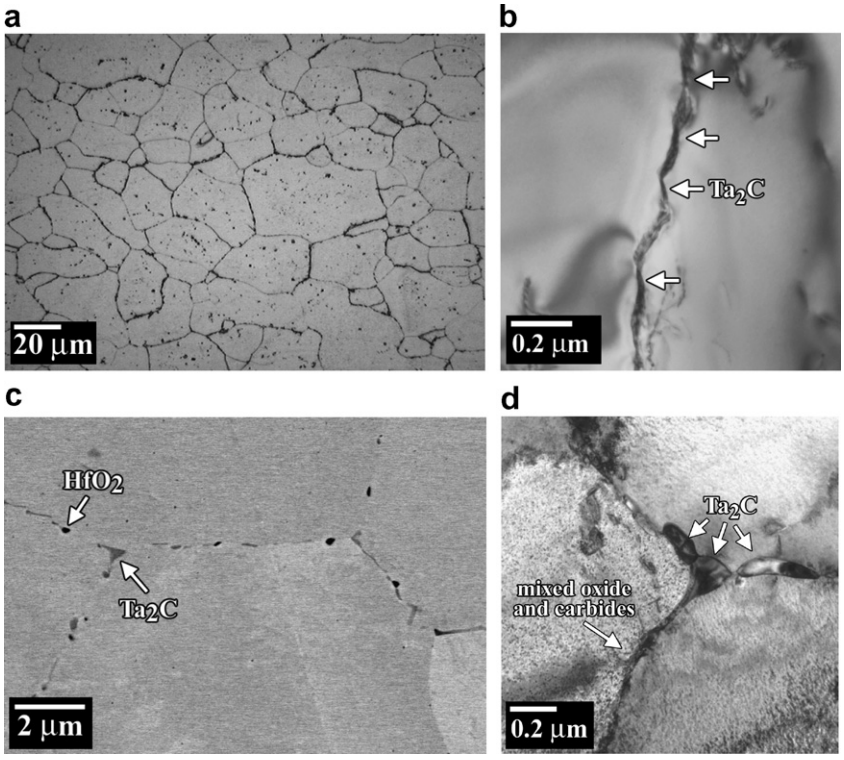


Fig. 10. Micrographs of ASTAR-811C. (a) OM of 1 h 1883 K annealed material, (b) TEM of 1100 h 1248 K aged material, (c) SEM and (d) TEM of 1100 h 1398 K aged material.

was also observed (Fig. 10(b)). The amount of carbide precipitation at the boundaries is difficult to estimate as it was not detectable under back-scatter imaging with the SEM. However, some boundaries examined under TEM showed a continuous carbide film between 10 and 20 nm thick for both the 1098 and 1248 K aging. In general and as shown in Fig. 10(b), the grain boundaries contained discrete carbides with a consistent orientation or habit to one of the parent grains, between which the grain boundary line was observed to kink or bow due to migration during aging. Aging at 1398 K resulted in similar intragranular carbides and oxides as in the lower temperature aging, but particles were fewer in number. However, the big difference between the 1398 K and the lower aging temperatures was in the size of the carbide particles along the grain boundaries. These particles, which were large enough to be clearly observed under back-scatter SEM imaging (Fig. 10(c)), were found to have grown preferentially into one of the adjacent grains at the boundary (Fig. 10(d)). A more detailed evaluation of the aged microstructures of ASTAR-811C will be presented in a separate paper.

The decrease in resistivity and hardness of ASTAR-811C with aging at 1098 and 1248 K may have been the result of interstitial elements precipitating out of the solid solution to form the oxide and carbide phases appearing intragranularly and along the grain boundaries of the material. This correlates with the tensile data (Table 7) showing a decrease in strength of the 1098 and 1248 K aged alloys compared to the as-annealed material tested under the same conditions. An increase in resistivity, hardness and yield strength was observed in the 1398 K aged material over that of the as-annealed condition. Though total elongation was still high in the 1398 K aged material, the reduction in uniform elongation may have been associated with the thicker grain boundary carbide development. The decrease in uniform elongation and increase in hardness at 1398 K may also be attributed to the increased oxygen and nitrogen levels in the material. The effect of interstitial impurities on the hardness of pure Ta has been investigated, with data compiled in references [24,25], and shows a linear increase in hardness occurring with the addition of O or N until saturation at levels of 3600 and 6600 wt ppm, respectively. Based on this data, a net increase of 430 wt ppm of O and N for the 1398 K aged material over the as-annealed represents only a minor increase in hardness and cannot alone justify the changes in mechanical properties.

The tensile properties of tantalum and tantalum-base alloys have been the focus of a number of research efforts. Senor and Horak compiled and evaluated the available experimental data and developed correlations for the physical properties of ASTAR-811C [26]. As these correlations were intended for use with space rector systems, Senor and Horak used only data which fit an established set of criteria. Specifically, they found that the data of Buckman and Goodspeed [27], Gold and Begley [28], Sheffler and Doble [29], and Gold and Lessman [30] 'agreed with each other reasonably well and fell into a band which should be typical of recrystallized

Table 7
Tensile properties of Ta-base alloys

| Alloy | Test temperature (K) | Condition | # of Tests | YS (MPa) | UTS (MPa) | Uniform elongation (%) | Total elongation (%) |
|---|---|---|---|---|---|---|---|
| ASTAR-811C | 295 | Annealed | 1 | 752 | 856 | 13.4 | 22.4 |
| | 1073 | Annealed | 1 | 331 | 642 | 12.5 | 18.9 |
| | | Aged 1098 K[a] | 3 | 295 | 546 | 13.5 | 20.2 |
| | 1223 | Annealed | 1 | 285 | 565 | 15.0 | 24.1 |
| | | Aged 1248 K[a] | 3 | 265 | 446 | 13.6 | 24.1 |
| | 1373 | Annealed | 1 | 309 | 516 | 13.7 | 24.5 |
| | | Aged 1398 K[a] | 3 | 363 | 487 | 9.0 | 20.4 |
| T-111 | 295 | Annealed | 1 | 699 | 787 | 15.4 | 29.2 |
| | 1073 | Annealed | 1 | 277 | 580 | 12.9 | 21.2 |
| | | Aged 1098 K[a] | 2 | 249 | 463 | 14.3 | 22.9 |
| | 1223 | Annealed | 1 | 269 | 523 | 15.2 | 26.4 |
| | | Aged 1248 K[a] | 2 | 231 | 459 | 11.2 | 20.5 |
| | 1373 | Annealed | 1 | 246 | 492 | 14.1 | 23.1 |
| | | Aged 1398 K[a] | 3 | 232 | 310 | 1.1 | 6.6 |

[a] Averaged values from multiple tests.

ASTAR-811C material'. The UTS of the annealed and aged ASTAR-811C of this study was in close agreement with the referenced data, while YS measured in this study was higher than those from literature, particularly at 1373 K.

Annealing the T-111 alloy for 1 h at 1883 K produced a uniform equiaxed grain structure, but contained a sparse, non-uniform distribution of $HfO_2$ particles. The mean grain diameter was on average 26 μm for all heat treatment conditions. The 0.3 μm $HfO_2$ particles from the annealing treatment were retained in the microstructures following all aging conditions. Examination of the 1098 K aged T-111 alloy (Fig. 11(a)) by electron microscopy methods revealed clean grain boundaries in the material. However, increases in aging temperature led to a progressive increase in the amount and size of precipitate formation along the grain boundaries. The back-scatter SEM image of the 1398 K aged microstructure, shown in Fig. 11(b), best exemplifies this change in precipitate development.

The gradual increase in precipitate formation in T-111 with increasing aging temperature correlates with the decreasing electrical resistivity and hardness values as more solute and interstitials precipitate out of solution. The increasing precipitate formation along the grain boundaries in T-111 produced a reduction in the tensile strengths of the aged material compared to the as-annealed, due to reduced solution hardening. However, the yield strengths of the as-annealed and aged material are within the scatter of earlier tests on T-111 based on correlations of the yield and ultimate tensile strength by Zinkle [31], from values reported by Wiffen [32], the Aerospace Structural Metals Handbook [22], and Tietz and Wilson [25] for T-111. The UTS measured for the annealed T-111 specimens of this study are slightly above the reported literature values, while values for the aged specimens at 1073 and 1223 K are quite close to the correlation curve. Although the oxygen content is slightly higher after aging at 1398 K than in the other conditions, with C and H content unchanged, the increased N content may have influenced the mechanical behavior of the specimens aged at 1398 K. However, it does not fully explain the extent of degradation of T-111 after aging. Indeed, all the aged specimens showed signs of degradation of tensile strength after aging, with the degree of degradation increasing with increasing aging temperature. However, there was no impurity pickup with aging at 1098 or 1248 K. The possibility also remains that the single value showing high N may be an anomaly or an artifact of material sampling for chemical analysis. Clear indications of solute segregation to the grain boundaries and the development of precipitates with increasing aging temperatures are apparent and have a detrimental affect on mechanical properties of the alloy. Reviews of literature on aged T-111 shows conflicting results on embrittlement. In work by Lessmann and Gold [5], no effect of aging on the bend test DBTT was observed for T-111 sheet aged under high vacuum between 1088 and 1588 K for up to 5000 h. Conversely, a decrease in bend test ductility was reported by Stephens [3] for T-111 tube annealed at 1925 K and aged 1000 h at 1315 K in either vacuum or lithium.

## 4. Conclusions

An evaluation of the microstructural changes resulting from 1100 h aging at 1098, 1248 and 1398 K was completed for candidate space-reactor

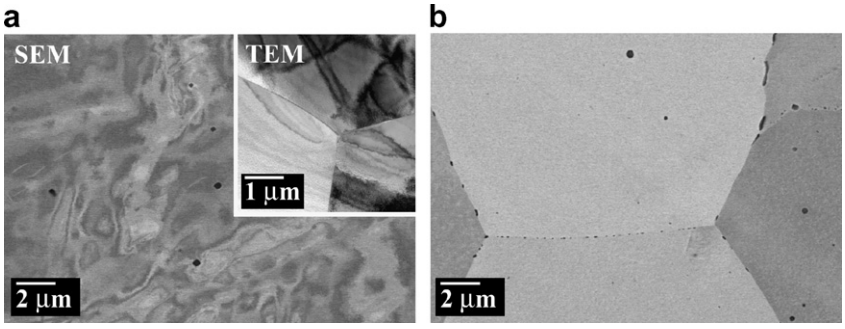


Fig. 11. Back-scatter electron SEM images of T-111 aged 1100 h at (a) 1098 K, with insert showing TEM image of grain boundary tri-junction, and (b) 1398 K.

refractory metal alloys, providing one of the first in-depth analyses of the phases present, their distribution and effect on electrical resistivity and mechanical properties. Aging for 1100 h resulted in changes in electrical resistivity from the as-annealed condition for most of the alloys investigated, indicating that some degree of microstructural evolution or solute redistribution had occurred during aging. Most of the aged materials showed measurable changes in mechanical properties compared to the as-annealed condition. Though slight or moderate increases in impurity concentration were observed for Mo–41Re, ASTAR-811C and T-111 alloys aged at 1398 K due to atmospheric contamination or an artifact in impurity analysis, the measured physical properties for these alloys are in agreement with the general trend observed in the alloy properties with increased aging temperature. The general changes in physical properties occurring in the aged material were found to correlate with the observed changes in the microstructures of the alloys.

No changes in microstructure or mechanical properties were found on aging the Mo–41Re alloy, with the material showing no evidence of precipitation. In contrast, the mechanical behavior of the Mo–47.5Re alloy was shown to be strongly influenced by the phases present at specific aging temperatures. The development of the σ phase along grain boundaries in material aged at 1398 K was detrimental to mechanical properties. Although similar grain boundary precipitation was observed for the χ phase at lower aging temperatures, the alloy did not show degraded mechanical properties. Issues related to notch sensitivity, corrosion, and fatigue are not known. In addition, longer aging times may lead to a further development of the grain boundary precipitates resulting in changes in mechanical properties.

Preliminary results on aged Nb–1Zr show that the precipitate development at different aging temperatures has a significant influence on electrical resistivity and mechanical properties and may show effects of particle overaging. The FS-85 and T-111 alloys exhibited signs of phase instability at grain boundaries during 1100 h aging at 1248 and 1398 K, respectively. Embrittlement of the alloys was associated with the precipitation of Zr or Hf compounds along grain boundaries. While marginally better performance was observed in the two alloys for the other aging temperatures as a result of different precipitate distributions on grain boundaries, longer aging times are needed to determine if embrittlement may also occur at these aging temperatures. Similarly, further work is required to understand the stability and effects of grain boundary carbide formation in ASTAR-811C and whether combinations of heat treatments can be used to control precipitation in the alloy.

## Acknowledgements

The authors thank J. Hack, R. Baranwal, T.M. Angeliu and Y. Ballout of the Naval Reactors Prime Contractor Team for many helpful technical discussions and guidance. The authors thank the following ORNL staff for their assistance on this Project: L.T. Gibson, D. Harper, R. Howell, J.W. Jones, J. Mayotte, J. McNabb, B. Sitterson, B. Sparks, K.A. Thomas and A.M. Williams in addition to C.E. Duty and F.W. Wiffen for their technical contributions. This work was performed under the sponsorship of NASA's Project Prometheus and directed by DOE/NNSA Naval Reactors. Opinions and conclusions drawn by the authors are not endorsed by DOE/NNSA Naval Reactors. Work on the Nb–1Zr alloy was sponsored by the Office of Fusion Energy Sciences, US Department of Energy. Research at the Oak Ridge National Laboratory SHaRE User center was sponsored by the Division of Materials Sciences and Engineering, US Department of Energy. ORNL is managed for DOE by UT-Battelle, LLC, under Contract DE-AC-05-00OR22725.

## References

[1] J.R. Stephens, Metallography 10 (1977) 1.
[2] J.R. Stephens, J. Less-Common Met. 51 (1977) 93.
[3] J.R. Stephens, Thermal aging effects in refractory metal alloys, in: M.S. El-Genk, M.D. Hoover (Eds.), Space Nuclear Power Systems, 1986, p. 291.
[4] G.K. Watson, J.R. Stephens, Effects of Aging at 1040 °C (1900 °F) on the Ductility and Structure of a Tantalum Alloy, T-111, NASA TN D-6988, NASA Lewis Research Center, Cleveland, OH, 1972.
[5] G.G. Lessmann, R.E. Gold, Thermal Stability of Refractory Metal Alloys, NASA-SP-245, Westinghouse Astronuclear Laboratory, Pittsburgh, PA, 1970.
[6] J.T. Busby, K.J. Leonard, L.L. Snead, F.W. Wiffen, S.J. Zinkle, J. Nucl. Mater., these Proceedings, doi:10.1016/j.jnucmat.2007.03.028.
[7] Standard Test Method for Resistivity of Electrical Conductor Materials, ASTM Designation B 193-87, ASTM Standards Online, American Society for Testing and Materials, Philadelphia, PA, 1992.

[8] A. Buch, Pure Metal Properties: A Scientific Technical Handbook, ASM International and Freund Publishing House Ltd., Materials Park, OH, 1999.
[9] Standard Test Method for Tension Testing of Metallic Materials, ASTM standard E8-04, ASTM Standards Online, American Society for Testing and Materials, Philadelphia, PA, 2001.
[10] (a) M. Li, D.T. Hoelzer, S.J. Zinkle, Electrical Resistivity Data of Vanadium Alloys in the RB-17J Experiment, Fusion Materials Semi-Annual Report, DOE/ER-0313/34, June, 2003, p. 2;
(b) S.J. Zinkle, A.N. Gubbi, W.S. Eatherly, Electrical Resistivity of V–Cr–Ti Alloys, Fusion Materials Semi-Annual Report, DOE/ER-0313/21, December, 1996, p. 15.
[11] K. Schroeder, CRC Handbook of Electrical Resistivities of Binary Metallic Alloys, CRC Press, Boca Raton, FL, 1983.
[12] T.B. Massalski (Ed.), Binary Alloy Phase Diagrams, vol. 2, ASM International, Metals Park, OH, 1986.
[13] Y. Nemoto, A. Hasegawa, M. Satou, K. Abe, Y. Hiraoka, J. Nucl. Mater. 324 (2004) 62.
[14] T. Leonhardt, J. Carlen, M. Buck, R. Weiju, C. Stevens, in: M.S. El-Genk (Ed.), Space Technology and Applications International Forum-STAIF 1999, American Institute of Physics, 458 (10) 1999, p. 685.
[15] J.A. Shields, in: M.S. El-Genk (Ed.), Space Technology and Applications International Forum-STAIF 2005, American Institute of Physics, 2005, p. 835.
[16] J.C. Carlen, B.D. Bryskin, J. Mater. Eng. Performance 32 (2) (1994) 282.
[17] K. Ogawa, R. Maddin, Acta Metall. Mater. 12 (1964) 1161.
[18] J.B. Lambert, 10 ed.Metals Handbook, vol. 2, ASM, 1990.
[19] L.J. Pionke, J.W. Davis, Technical Assessment of Niobium Alloys Data Base for Fusion Reactor Applications, US Department of Energy Report, C00-4247-2, August, 1979.
[20] T.A. Moss, Nucl. Appl. 3 (1967) 71.
[21] R.G. Frank, Recent Advances in Columbium Alloys, AIME Symposium on Metallurgy and Technology of Refractory Metal Alloys, Washington, DC, The Metallurgical Society of AIME, Plenum, New York, NY, 1968, p. 325.
[22] D.C. Goldberg, in: W.F. Brown, S.J. Setlak (Eds.), Aerospace Structural Metals Handbook, 37 ed., CINDAS/USAF CRDA Handbooks Operation, Purdue University, West Lafayette, IN, 2001.
[23] R.L. Ammon, R.W. Buckman, D.L. Harrod, Development of Advanced High Strength Tantalum Base Alloys, Phase III-Influence of Metallurgical Condition on the Mechanical Properties of ASTAR-811C Sheet, Westinghouse Astronuclear Laboratory, Report NASA-CR-121096/WANL-M-FR-72-009, Pittsburgh, PA, December, 1972.
[24] W.D. Wilkinson, Properties of Refractory Metals, Gordon and Breach Science Publishers Inc., New York, NY, 1969.
[25] T.E. Tietz, J.W. Wilson, Behavior and Properties of Refractory Metals, Stanford University, Stanford, CA, 1965.
[26] D.J. Senor, J.A. Horak, Material Property Correlations for W–25Re, Mo–50Re and ASTAR-811C, unpublished, 1989, p. 1.
[27] R.W. Buckman Jr., R.C. Goodspeed, in: I. Machlin, R.T. Begley, E.D. Weisert (Eds.), Refractory Metal Alloys Metallurgy and Technology, Plenum, New York, NY, 1968, p. 373.
[28] R.E. Gold, R.T. Begley, Investigation of High Temperature Fracture of T-111 and ASTAR-811C, NASA-CR-72859, Westinghouse Astronuclear Laboratory, Pittsburgh, PA, 1971.
[29] K.D. Sheffer, G.S. Doble, Influence of creep damage on the low cycle thermal–mechanical fatigue behavior of two tantalum-base alloys, NASA-CR-121001, 1972.
[30] R.E. Gold, G.G. Lessmann, The Influence of Restrain and Thermal Exposure on Welds in T-111 and ASTAR-811C, NASA-CR-72858, Westinghouse Astronuclear Laboratory, Pittsburgh, PA, 1971.
[31] S.J. Zinkle, Thermophysical and mechanical properties for Ta-8%W-2%Hf, Fusion Materials Semi-Annual Report, DOE/ER-0313/27, December, 1999, p. 175.
[32] F.W. Wiffen, in: R.J. Arsenault (Ed.), Proceedings of the International Conference on Defects and Defect Clusters in BCC Metals and Their Alloys, Nuclear Metallurgy, vol. 18, National Bureau of Standards, 1973, p. 176.